J. Fluid Mech. (2020), *vol.* 885, A1. © Cambridge University Press 2019
doi:10.1017/jfm.2019.982

General exotic capillary tubes

Fei Zhang[1,2] **and Xinping Zhou**[1,†]

[1]School of Mechanical Science and Engineering, Huazhong University of Science and Technology, Wuhan 430074, PR China

[2]Department of Mechanics, Huazhong University of Science and Technology, Wuhan 430074, PR China

(Received 24 July 2019; revised 19 October 2019; accepted 20 November 2019)

The general exotic capillary tube is a non-uniform capillary tube which permits an entire continuum of equilibrium menisci if applying a pressure $p = -\varepsilon z$ at the tube inlet. The shapes of general exotic capillary tubes under positive and negative loads are determined mathematically. Lowering the pressure at the tube inlet slightly from the value $p = -\varepsilon z$ causes the tube to completely drain out, while raising the pressure slightly forces the tube to fill up, which implies that the general exotic capillary tube is sensitive to pressure. The general exotic capillary tube is also related to meniscus stability. It is found that the boundary parameters χ_1 of general exotic cylinders with arbitrary contact angle are equal to the critical values χ_1^* for determining the meniscus stability. Then, a convenient alternative to solving the Jacobi equation for determining χ_1^* is proposed based on the 'exotic' property.

Key words: capillary flows

1. Introduction

Numerous natural systems contain narrow spaces that enable liquid transport, such as porous media (e.g. Wang & Cheng 1996). This behaviour, called capillary action, occurs because of the combination of surface tension and adhesive forces between liquid and solid. A typical example is the rise of a liquid in a capillary tube vertically positioned in an infinite liquid. From the aspect of statics, previous studies have been conducted to examine the shapes of equilibrium menisci dating back to the nineteenth century (Young 1805). It is known that the meniscus in a uniform circular tube can be uniquely determined by the contact angle and the tube radius. However, a non-uniform circular tube (i.e. an axisymmetric tube with a variable radius) may admit two or more equilibrium menisci (e.g. Finn 1988; Tsori 2006). Except in a few cases, the uniqueness of menisci cannot always be expected (Finn 1988).

Motivated by the non-uniqueness of menisci, an axisymmetric container (called the exotic container) which permits an entire continuum of equilibrium menisci was proposed and studied theoretically (Gulliver & Hildebrandt 1986; Finn 1988; Concus & Finn 1989, 1991). The exotic container is determined mathematically so that all the menisci have the same potential energy and bound the same volume of liquid. However, these axisymmetric menisci turn out to be unstable (i.e. none of them is a

† Email address for correspondence: xpzhou08@hust.edu.cn

local minimizer of energy) (Finn 1988; Concus & Finn 1989; Wente 1999), which leads to the prediction that there are non-axisymmetric menisci with a local minimum of energy in the exotic container. However, there is at present no known way to determine the non-axisymmetric menisci theoretically in the exotic container. Using the Surface Evolver software (Brakke 1992), the non-axisymmetric menisci were found numerically by Callahan, Concus & Finn (1991). Results showed that there are three distinct non-axisymmetric menisci in the exotic container. However, only two non-axisymmetric menisci were observed experimentally (Concus, Finn & Weislogel 1992, 1999). The loss of axisymmetry (i.e. the non-axisymmetric instability) is not an exclusive phenomenon for the exotic container. Non-axisymmetric instability can occur even if conditions for an exotic container are not entirely met (Concus *et al.* 1999) and can also be observed for a liquid bridge when the Steiner limit is exceeded (Gillette & Dyson 1972; Russo & Steen 1986; Slobozhanin, Alexander & Resnick 1997). Though the non-axisymmetric menisci, in general, cannot be determined mathematically, the stability analysis of menisci can allow one to obtain the critical conditions for the onset of non-axisymmetric instability. A comprehensive review of the stability of menisci has been presented by Bostwick & Steen (2015).

Inspired by the exotic container, Wente (2011) extended the 'exotic' property to a capillary tube and proposed a non-uniform circular tube, called the exotic capillary tube (ECT), vertically positioned in an infinite liquid which permits an entire continuum of equilibrium menisci. Following Wente (2011), Zhang & Zhou (2020) investigated the interior, exterior and planar cases of ECTs together (collectively called the exotic cylinder), and then examined their stabilities by the method of Slobozhanin & Alexander (2003). Results showed that each of the menisci for the exotic cylinder has the smallest eigenvalue $\lambda_{01} = 0$ to axisymmetric perturbations and the menisci are stable, in contrast to the case of the exotic container. This is because the stability is sensitive to the constraint on the liquid. The eigenvalue λ is associated with the second variation of energy and $\lambda < 0$ corresponds to instability. For the exotic containers, only volume-preserving variations (called volume disturbances) of the interface are allowed because there is a volume constraint. However, for the exotic cylinders, there is no volume constraint restricting the variations (called pressure disturbances). For an axisymmetric problem, both pressure and volume disturbances consist of axisymmetric perturbations and non-axisymmetric perturbations, where non-axisymmetric perturbations satisfy the volume constraint automatically (i.e. no added volume constraint is enforced on non-axisymmetric perturbations even for the constrained problem) (Myshkis *et al.* 1987).

Then, we discuss why the axisymmetric menisci in the exotic containers are unstable to non-axisymmetric perturbations while the axisymmetric menisci in the exotic cylinders are stable. The 'exotic' property indicates that the axisymmetric menisci have the smallest eigenvalue $\lambda_{01} = 0$ to axisymmetric perturbations for the exotic containers and the exotic cylinders (see Wente 1999; Zhang & Zhou 2020). Myshkis *et al.* (1987) have shown that for an unconstrained axisymmetric problem one has $\lambda_{01} < \lambda_{11}$, where λ_{11} is the smallest eigenvalue to non-axisymmetric perturbations, which means that the unconstrained axisymmetric meniscus to axisymmetric perturbations is less stable than to non-axisymmetric perturbations. Thus, the unconstrained axisymmetric menisci for the exotic cylinder are stable and have the smallest eigenvalue $\lambda_{01} = 0$ to pressure disturbances. For a constrained axisymmetric problem, $\min(\lambda_{01}, \lambda_{11})$ is, in general, the smallest eigenvalue, and λ_{11} is the smallest eigenvalue in the case of simply connected menisci with Bond number $Bo > 0$ (Myshkis *et al.* 1987). Then we have $\lambda_{11} < \lambda_{01} = 0$ for the exotic

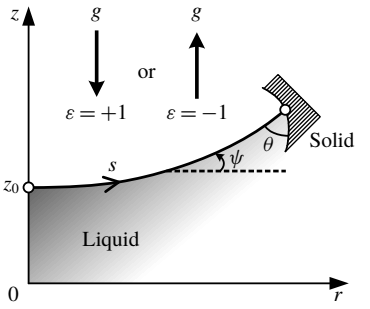

FIGURE 1. Profile of a meniscus meeting a solid at a contact angle θ under gravity g. There are two directions of gravity: the downward and upward directions corresponding to positive loads $\varepsilon = +1$ and negative loads $\varepsilon = -1$, respectively. The meniscus is simply connected when the meniscus touches the axis of symmetry $r = 0$. The case of an unconstrained liquid is considered and the water line is fixed at $z = 0$ so that the pressure difference $\Delta p = -\varepsilon z$.

container, and therefore the menisci are unstable to non-axisymmetric perturbations. This conclusion was also drawn by Wente (1999) by examining the second variation of energy of the planar meniscus in the exotic container to all gravity levels. It was found that the infimum of the second variation of energy is less than zero. This can also be explained in that the axisymmetric planar menisci (which are assumed to exist in the exotic container) always have the relations $\lambda_{01} > \lambda_{11}$ for all values of the Bond number (see Myshkis *et al.* 1987, pp. 140–143) and $\lambda_{01} = 0$ due to the 'exotic' property.

The ECTs discussed above studied by Wente (2011) and Zhang & Zhou (2020) need to be vertically positioned correctly in an infinite liquid under positive loads (gravity down into the liquid) to have the 'exotic' property. To ensure the ECT is in contact with the infinite liquid, there must be an axisymmetric planar meniscus in the ECT. For negative loads, to our knowledge, the infinite liquid cannot be stable, though the corresponding ECT shapes can be determined mathematically. To make the ECTs under negative loads physically meaningful, we set an appropriate constant pressure at the inlet of the ECT (called a general ECT) instead of placing the ECT in an infinite liquid even though the above two considerations are in a sense the same mathematically. Thus, there will not necessarily be an axisymmetric planar meniscus in the general ECT and the general ECT shapes can be determined under positive and negative loads. Meanwhile, the stability analysis of axisymmetric menisci in ECTs can be also extended to the case of negative loads.

2. Theory

We describe the configuration of an unconstrained axisymmetric liquid partially wetting a solid using the notation shown in figure 1. By introducing cylindrical coordinates (r, z) with the origin located at the water line, r is the radius from the axis of symmetry and z is the height of the meniscus from the water line. The meniscus profile is represented by the parameterized curve $(r(s), z(s))$ by the introduction of its arc length s. We scale all lengths by the capillary length $l = \sqrt{\sigma/\rho g}$, curvature by l^{-1} and pressure by $\rho g l$, where σ is the surface tension of the interface, ρ is the density difference between the two fluids and g is the gravitational acceleration.

2.1. *Family of solution curves*

As shown in figure 1, there are two directions of gravity for the configuration: the downward and upward directions corresponding to positive loads $\varepsilon = +1$ and negative loads $\varepsilon = -1$, respectively. It is well known that the profile of the equilibrium meniscus is governed by the Young–Laplace equation, which can be expressed in parametric form (see e.g. Huh & Scriven 1969; Boucher & Evans 1975; Finn 1986):

$$\frac{\mathrm{d}r}{\mathrm{d}s} = \cos\psi, \quad \frac{\mathrm{d}z}{\mathrm{d}s} = \sin\psi, \quad \frac{\mathrm{d}\psi}{\mathrm{d}s} = \varepsilon z - \frac{\sin\psi}{r}, \tag{2.1a–c}$$

where ψ is the inclination angle of the meniscus. The initial conditions for the simply connected meniscus are

$$r = 0, \quad z = z_0 \quad \text{at } s = 0. \tag{2.2a,b}$$

In practice, the solutions of the linearized Young–Laplace equation $r^2 z'' + rz' - \varepsilon r^2 z = 0$ (valid at small inclination angles) satisfying (2.2) (Siegel 1980; Finn 1986),

$$z = \tan\psi^* \mathrm{I}_0(r)/\mathrm{I}_1(r^*), \quad \text{for } \varepsilon = +1, \tag{2.3a}$$

$$z = -\tan\psi^* \mathrm{J}_0(r)/\mathrm{J}_1(r^*), \quad \text{for } \varepsilon = -1, \tag{2.3b}$$

are used to determine the initial conditions to avoid the singularity of (2.1*c*) at $r = 0$, where J (I) are the (modified) Bessel functions of the first kind, the subscripts '0' and '1' indicate the orders of the (modified) Bessel functions and r^* and ψ^* are the parameters of the solution curve. Arbitrarily choosing a value of r^* and a small value of ψ^*, a solution curve for $0 \leqslant r \leqslant r^*$ is determined by (2.3). Then substituting $r = r^*$ into (2.3) gives the initial conditions $(r, z, \psi) = (r^*, z^*, \psi^*)$ for (2.1). The appropriate value of ψ^* can be chosen as $+0.01^\circ$, leading to $z^* \approx z_0$. The cases of $\psi^* = -0.01^\circ$ can be determined easily because of the symmetry with respect to $z = 0$.

Integrating (2.1) with the initial conditions (r^*, z^*, ψ^*) for a set of values of r^* and $\psi^* = 0.01^\circ$, two families of solution curves under positive and negative loads are determined, as shown in figure 2. The solution curves for $\varepsilon = +1$ can also be determined by integrating a different parametric form of the Young–Laplace equation (see e.g. Zhang & Zhou 2020), where the parameter is not the arc length s but the inclination angle ψ. However, this parametric form is not suitable for the case of $\varepsilon = -1$, because of the singularity of $(\mathrm{d}/\mathrm{d}\psi)$ (i.e. the curvature $\mathrm{d}\psi/\mathrm{d}s = 0$) at the inflection points (e.g. the red point in figure 2*b*).

In figure 2(*a*,*b*), a pair (ψ, z_0) can be uniquely determined by its coordinates (r, z) in the regions Λ_1 and Λ_2 (Wente 2011), because the coordinates (r, z) can uniquely determine a solution curve and an inclination angle in Λ_1 and Λ_2. These two regions (grey shaded areas) in the quadrant of the r–z plane are bounded by the coordinate axes and the envelopes (ζ_1 and ζ_2 in figure 2). In these regions, the Jacobian determinants of $(r(\psi, t), z(\psi, t))$,

$$F = \frac{\partial r}{\partial \psi}\frac{\partial z}{\partial t} - \frac{\partial r}{\partial t}\frac{\partial z}{\partial \psi}, \tag{2.4}$$

are non-zero and keep the same sign (Finn 1986; Wente 2011). The vanishing of F locates the envelopes ζ_1 and ζ_2. As shown in figure 2(*a*), the envelope ζ_1 is represented by a function $z = e_1(r)$, decreasing with r with $\lim_{r\to 0^+} e_1(r) = +\infty$ and $\lim_{r\to+\infty} e_1(r) = 2$ (Wente 2011). In figure 2(*b*), the envelope ζ_2 is represented by a

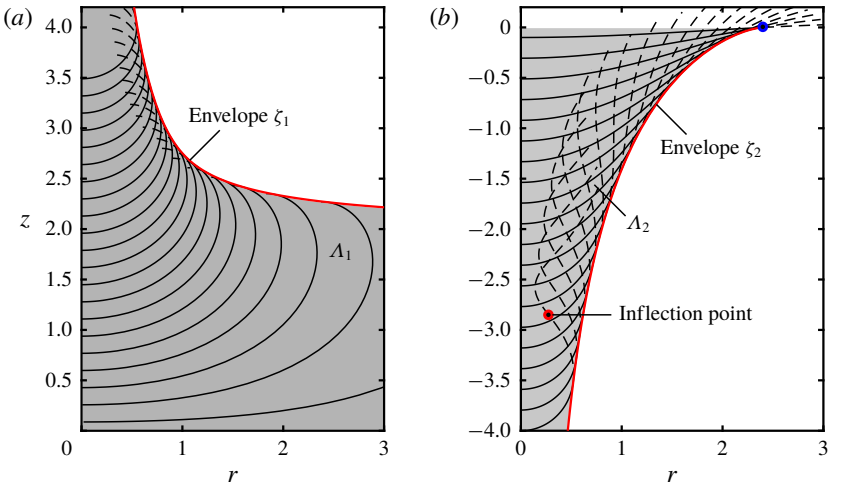

FIGURE 2. Two families of solution curves for (2.1): (*a*) $\varepsilon = +1$ for $\psi \in [0, \pi]$ and (*b*) $\varepsilon = -1$ for $s \in [0, 3]$. The shaded areas Λ_1 and Λ_2 represent the maximal stability regions. The black lines are the solution curves, which are divided by the envelopes into two parts: the lower part is denoted by the solid line in the maximal stability regions and the upper part is denoted by the dashed line. The blue point $(r_0, 0)$ is the endpoint of the envelope ζ_2.

function $z = e_2(r)$, increasing with r with $\lim_{r\to 0^+} e_2(r) = -\infty$ and $e_2(r_0) = 0$ (see the blue point). The endpoint $(r_0, 0)$ of ζ_2 can be determined by the asymptotic solution of the Young–Laplace equation $G(z, r, t) = z - t\mathrm{J}_0(r) = 0$, i.e. (2.3*b*). By substituting the asymptotic solution into $\partial G/\partial t = 0$ for determining the envelope (Lawrence 2013), we have $\mathrm{J}_0(r_0) = 0$, where $r_0 \approx 2.405$ is the first zero of $\mathrm{J}_0(r)$.

Zhang & Zhou (2020) have shown that the envelopes ζ_1 and ζ_2 are closely related to meniscus stability. It is known that an envelope of a family of curves is defined as a curve that touches every member of the family tangentially (Lawrence 2013). The envelopes also bound the maximal stability regions (Λ_1 and Λ_2) which correspond to the maximal possible profiles of stable menisci, called the maximal stable profiles by Slobozhanin & Alexander (2003). This means that only the meniscus in Λ_1 and Λ_2 is likely to be stable, for reasons discussed in § 3.2. Therefore, the points on the envelope are conjugate points of the Jacobi equation, i.e. the instability points. This can be explained in that the envelopes can be regarded as ECTs with zero contact angle, and the menisci in the ECTs correspond to the instability points to pressure disturbances (Zhang & Zhou 2020). This implies that the shape of the ECT is closely related to meniscus stability. In the calculus of variations, a similar fact is that if a family of extremals to a functional through a fixed point has an envelope, then a point where an extremal intersects the envelope is a conjugate point to the fixed point (see e.g. Gulliver & Hildebrandt 1986).

2.2. *Determination of the shape of ECTs*

The shape of the ECT with contact angle θ is the integral curve of the slope field $\{\cos(\psi + \theta), \sin(\psi + \theta)\}$, where the scalar fields $\psi(r, z)$ for $\varepsilon = \pm 1$ are determined in the regions Λ_1 and Λ_2, respectively (see figure 2) (Wente 2011). Meanwhile, we know that the integral curve of the slope field $\{\cos\psi, \sin\psi\}$ is the solution curve of

the Young–Laplace equation. Thus, following the parametric form (2.1*a–c*), we can construct

$$\left.\frac{\mathrm{d}x}{\mathrm{d}s}\right|_S = \cos(\psi+\theta), \quad \left.\frac{\mathrm{d}y}{\mathrm{d}s}\right|_S = \sin(\psi+\theta), \quad \left.\frac{\mathrm{d}\psi}{\mathrm{d}s}\right|_S = \tilde{K}(x, y; \theta) \tag{2.5a–c}$$

to determine the ECT, where (x, y) denotes a point on the generatrix of the ECT in the r–z plane, $\tilde{K}(x, y; \theta)$ is the curvature of the integral curve of $\{\cos(\psi+\theta), \sin(\psi+\theta)\}$ ($\tilde{K} < 0$ if the solid is convex to the liquid) and $(\mathrm{d}/\mathrm{d}s)|_S$ denotes the directional derivative along the solid surface, i.e. in the direction $(\cos(\psi+\theta), \sin(\psi+\theta))$.

Then we have

$$K = \left.\frac{\mathrm{d}\psi}{\mathrm{d}s}\right|_L = \psi_r \cos\psi + \psi_z \sin\psi, \tag{2.6a}$$

$$\tilde{K} = \left.\frac{\mathrm{d}\psi}{\mathrm{d}s}\right|_S = \psi_r \cos(\psi+\theta) + \psi_z \sin(\psi+\theta), \tag{2.6b}$$

where K is the curvature of the integral curve of $\{\cos\psi, \sin\psi\}$, the subscripts r and z denote the partial derivatives and $(\mathrm{d}/\mathrm{d}s)|_L$ denotes the directional derivative along the liquid surface, i.e. in the direction $(\cos\psi, \sin\psi)$. Therefore, the partial derivatives ψ_r and ψ_z are related by

$$\psi_r \cos\psi + \psi_z \sin\psi = \varepsilon z - \frac{\sin\psi}{r}. \tag{2.7}$$

Once ψ_r or ψ_z is determined, $\tilde{K}$ in (2.5*c*) is determined by (2.6*b*), and then the shape of the ECT is obtained by integrating (2.5).

The partial derivative ψ_r can be calculated by integrating (2.1) together with

$$\left.\frac{\mathrm{d}\psi_r}{\mathrm{d}s}\right|_L = \frac{\sin\psi}{r^2} + \frac{\psi_r(\psi_r - \varepsilon z\cos\psi)}{\sin\psi}. \tag{2.8}$$

The derivation of (2.8) is shown in appendix A. To determine $\tilde{K}$, the boundary conditions for (2.1) and (2.8) are

$$r(0) = 0, \quad \psi(0) = 0 \quad \text{and} \quad r(s_1) = x, \quad z(s_1) = y. \tag{2.9a,b}$$

In summary, there are two systems to be solved for the shapes of the ECTs. The first system consists of the initial-value problem: equations (2.5) with appropriate initial conditions, where $\tilde{K}(x, y; \theta)$ is determined by solving the second system. The second system consists of the boundary-value problem: equations (2.1) and (2.8) with the boundary conditions (2.9).

The second system is solved here by the shooting method. Equation (2.1) is integrated first, using (2.9*a*) and a guessed value of $z(0)$ as initial conditions, until $r = x$. At this point, the boundary condition $z = y$ is generally not satisfied. Then, the value of $z(0)$ is adjusted by the secant method and this process is repeated until $z = y$ is satisfied to the desired accuracy. Thus, the appropriate value of $z(0)$ is found to accommodate the boundary conditions (2.9). Then, we integrate (2.1) and (2.8), using $(\psi, r, z) = (0, 0, z(0))$ and the value of ψ_r at the point $(0, z(0))$ as initial conditions, to obtain the value of ψ_r at $(x(s_1), y(s_1))$. Finally, $\tilde{K}(x, y; \theta)$ is determined by (2.6*b*) and (2.7).

In the above computations, to avoid the singularity of (2.1) and (2.8) at $r=0$, the asymptotic solutions (2.3) are used for determining the initial conditions (ψ^*, r^*, z^*) at $s=r^*$ (due to small inclination angles), where the value of ψ^* is chosen as $+0.01°$. The initial condition for ψ_r is determined by differentiating (2.3) with r^* and ψ^* replaced, respectively, by r and ψ with respect to r.

2.3. *Relation to meniscus stability*

As discussed in § 1, the unconstrained axisymmetric meniscus is less stable to axisymmetric perturbations than to non-axisymmetric perturbations (i.e. $\lambda_{01} < \lambda_{11}$). Thus, only axisymmetric perturbations are considered in this section. Because the meniscus is unconstrained, the meniscus stability is with regard to pressure disturbances. Following the method described by Slobozhanin & Alexander (2003), the stability of the configuration in figure 1 is investigated by solving the Jacobi equation in the axisymmetric case:

$$-\varphi_0'' - \frac{r'}{r}\varphi_0' + a(s)\varphi_0 = 0, \tag{2.10}$$

with

$$a(s) \equiv \cos\psi - K^2 - \frac{\sin^2\psi}{r^2}, \tag{2.11}$$

and the initial conditions

$$\varphi_0(0) = 1, \quad \varphi_0{}'(0) = 0. \tag{2.12a,b}$$

The points letting $\varphi_0(s_c) = 0$ are conjugate points on the boundaries of the regions Λ_1 and Λ_2, i.e. the envelopes of the solution curves (see figure 2). In Λ_1 and Λ_2, the boundary parameter of the solid (figure 1) is defined as

$$\chi_1 \equiv \frac{K(s_1)\cos\theta - \tilde{K}}{\sin\theta}, \tag{2.13}$$

where $K(s_1)$ is the curvature of the meniscus profile at which the meniscus meets the solid. The critical value of χ_1 is calculated by

$$\chi_1^* = -\frac{\varphi_0{}'}{\varphi_0}. \tag{2.14}$$

By comparing the boundary parameter χ_1 and its critical value χ_1^*, the stability of menisci to pressure disturbances is determined: the equilibrium within the regions Λ_1 and Λ_2 is stable if $\chi_1 > \chi_1^*$, and is unstable if $\chi_1 < \chi_1^*$ (Slobozhanin & Alexander 2003). For a fixed meniscus shape, the meniscus stability is sensitive to the boundary conditions for the disturbance. For free disturbances (with a free contact line), we conclude from (2.13) that a convex solid ($\tilde{K} < 0$) is relatively stable to a planar solid ($\tilde{K} = 0$), which is relatively stable to a concave solid ($\tilde{K} > 0$). For pinned disturbances (with a fixed contact line), the meniscus is in contact with a sharp solid edge (i.e. $\tilde{K} \to -\infty$) and therefore the meniscus has the boundary parameter $\chi_1 \to \infty$. If the meniscus is in the maximal stability regions Λ_1 and Λ_2, the meniscus with $\chi_1 \to \infty$ is stable.

The ECT has the boundary parameter $\chi_1 = \chi_1^*$ corresponding to each meniscus because of its 'exotic' property, as discussed in § 1. We have verified that $\chi_1 = \chi_1{}^*$ for exotic cylinders with $\varepsilon = +1$ by numerically solving (2.10) in a previous study (Zhang & Zhou 2020). The Jacobi equation (2.10) for $\varepsilon = +1$ is numerically solved using the spectral parameter power series method (Kravchenko & Porter 2010), which expresses the general solution of the Sturm–Liouville equation as a spectral parameter power series.

Substituting (2.6) into (2.13), we obtain the boundary parameter of the ECT:

$$\chi_1 = \chi_1^* = \psi_r \sin\psi - \psi_z \cos\psi, \tag{2.15}$$

where ψ_r and ψ_z are determined as in § 2.2. This relation provides a convenient method for calculating the critical value χ_1^* of the boundary parameter for a simply connected axisymmetric meniscus without solving the Jacobi equation (2.10). This method was proposed earlier for $\varepsilon = +1$ in Zhang & Zhou (2020), where the parameter is the inclination angle ψ instead of the arc length s in this work.

There is also a rich geometry surrounding the critical value $\chi_1{}^*$, which is closely related to the curvature $\tilde{K}_N$ of the generatrix of the ECT with $\theta = \pi/2$:

$$\chi_1^* = -\tilde{K}_N, \tag{2.16}$$

which can be easily derived by substituting $\theta = \pi/2$ into (2.6*b*) or (2.13). From (2.13), we can see that the boundary parameter χ_1 is related to the contact angle θ, the curvature K of the meniscus and the curvature $\tilde{K}$ of the solid. However, from (2.15) we have that the critical value χ_1^* is independent of θ and can be determined uniquely by its location (r, z) and ε. Thus, if two different ECTs with different contact angles under the same loads have an intersection point (r, z), their boundary parameters will be equal at the point (r, z).

3. Results and discussion

Using appropriate initial conditions for the mathematical model described in § 2.2, the general ECTs are determined and investigated. Then the critical values χ_1^* of the boundary parameters are calculated using the method proposed in § 2.3 for the configuration in figure 1.

3.1. *General ECTs*

Wente (2011) investigated ECTs that permit a flat disc-shaped meniscus. These ECTs are proposed under the consideration that the ECTs are positioned in an infinite liquid bath under positive loads (i.e. the case of $\varepsilon = +1$ in figure 1), and the ECT shapes are parts of the entire integral curves of $\{\cos(\psi + \theta), \sin(\psi + \theta)\}$ for $\varepsilon = +1$. Following Wente (2011), we consider a non-uniform circular capillary tube (called a general ECT) with a specific shape that has constant pressure at the inlet and also permits an entire continuum of equilibrium menisci in itself. Thus, each integral curve for $\varepsilon = +1$ and $\varepsilon = -1$ corresponds to a general ECT.

Figure 3(*a–d*) shows the integral curves (black thick lines) of the slope fields $\{\cos(\psi + \theta), \sin(\psi + \theta)\}$ for $\varepsilon = +1$, -1 and $\theta = 45°$, $90°$. These integral curves intersect the menisci (thin lines) at a constant angle θ (i.e. the 'exotic' property). In figure 3(*a*,*b*), the integral curves for $\varepsilon = +1$ and $\theta = 45°$, $90°$ can be divided into five types depending on the number and locations of the endpoints: (i) one endpoint is

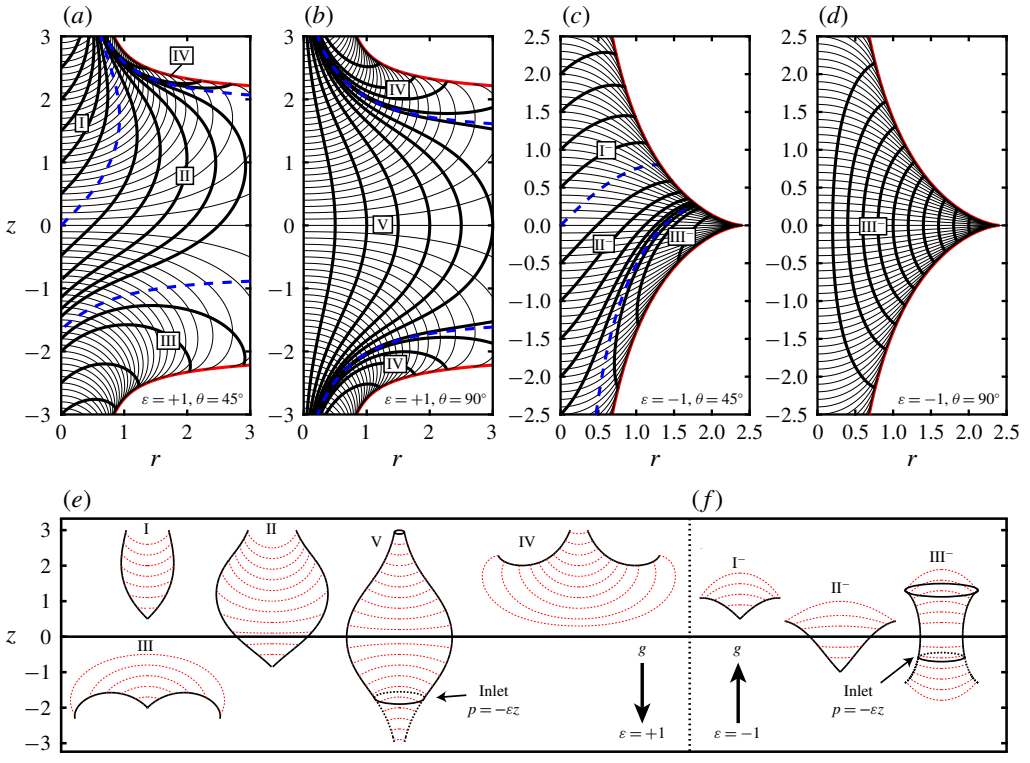

FIGURE 3. Integral curves of $\{\cos(\psi+\theta), \sin(\psi+\theta)\}$ (thick lines) and $\{\cos\psi, \sin\psi\}$ (thin lines): (*a*) $\varepsilon=+1$, $\theta=45°$; (*b*) $\varepsilon=+1$, $\theta=90°$; (*c*) $\varepsilon=-1$, $\theta=45°$; (*d*) $\varepsilon=-1$, $\theta=90°$. There are five types of integral curves for $\varepsilon=+1$ (*a*,*b*) and three types of integral curves for $\varepsilon=-1$ (*c*,*d*). The regions of integral curves of different types are separated by their boundaries (blue dashed lines). Typical general ECT shapes (black solid lines) for (*e*) $\varepsilon=+1$ and (*f*) $\varepsilon=-1$ are depicted, which intersect the menisci (red dashed lines) at a constant angle θ.

on the positive half-axis of z (region I); (ii) one endpoint is on the negative half-axis of z (region II); (iii) two endpoints are on the negative half-axis of z and the lower envelope (red thick line), respectively (region III); (iv) one endpoint is on an envelope (region IV); and (v) there is no endpoint (region V). The integral curves in II and V which have been studied by Wente (2011) intersect the r axis and correspond to the ECTs that permit a flat disc-shaped meniscus. The integral curves in V which have no endpoint appear only when $\theta=90°$. In I, III and IV, the integral curves do not intersect the r axis and the corresponding ECTs are connected to a liquid which has a constant pressure at the inlet, rather than are vertically positioned in an infinite bath, to process the 'exotic' property (see figure 3*e*). Therefore, these general ECTs, extended from the ordinary ECTs studied by Wente (2011), can be seen as non-uniform circular nozzles connected to a liquid bath which has a constant pressure at the inlet. The general ECTs can also be constructed under negative loads ($\varepsilon=-1$), as shown in figure 3(*c*,*d*,*f*). The integral curves for $\varepsilon=-1$ and $\theta=45°$, 90° can be divided into three types depending on the number and locations of their endpoints: (i) two endpoints are on the positive half-axis of z and the upper envelope, respectively (region I$^-$); (ii) two endpoints are on the negative half-axis of z and

the upper envelope, respectively (region II$^-$); and (iii) two endpoints are on two envelopes, respectively (region III$^-$). Only the curves in region I$^-$ do not intersect the r axis. The above classifications for $\theta = \pi/4$ can be extended to the case $\theta \in (0, \pi/2)$. The supplementary cases of $\pi - \theta$ can be obtained by reflecting the cases of θ about $z = 0$.

In the study of Wente (2011), the ordinary ECTs (in II and V) have a surprising behaviour whereby lowering the ECT slightly from its natural position (as shown in figure 3*e*) causes the ECT to completely fill up, while raising the ECT slightly forces the ECT to drain out. Wente (2011) proved the above results by comparing the energies, $E(\Omega_1)$ and $E(\Omega)$, of the configurations with a meniscus Ω_1 (the profile of which is the integral curve of $\{\cos\psi, \sin\psi\}$ and meets the ECT at a contact angle θ_t) and an admissible meniscus Ω, where the ECT has a natural contact angle θ_n. Here the contact angle θ_t denotes the intersection angle between the meniscus and the ECT and may not equal θ_n. It was found that $E(\Omega_1) < E(\Omega)$ when $\theta_t < \theta_n$ and Ω lies above Ω_1 (or when $\theta_t > \theta_n$ and Ω lies below Ω_1). Wente (2011) also showed that if the ECT with contact angle θ_n is shifted upward then the new contact angle θ_t will satisfy $\theta_t < \theta_n$, and if the tube is shifted downward then we will have $\theta_t > \theta_n$. Therefore, when raising the ECT slightly, there is always a meniscus with $\theta_t < \theta_n$ and a lower energy below any admissible meniscus, which implies that the fluid is unable to remain inside the ECT and must flow out. An analogous situation that the fluid fills up the ECT occurs when lowering the ECT slightly.

Motivated by the above observations, the general ECTs also have a similar behaviour whereby lowering the pressure at the ECT inlet slightly from the value $p = -\varepsilon z$ causes the ECT to completely drain out, while raising the pressure slightly forces the ECT to fill up. This is because raising and lowering the pressure are equivalent to lowering and raising the ECT for the case of $\varepsilon = +1$, respectively. We note that the shifted ECT (e.g. in region III in figure 3*a*) may not locate in the extremal field (bounded by two envelopes and the z axis) and the meniscus on the part not in the extremal field is always unstable and has a higher energy. Thus, the above results can be extended to the case of $\varepsilon = +1$. For the case of $\varepsilon = -1$, raising the pressure is equivalent to raising the ECT, while lowering the pressure corresponds to lowering the ECT. Contrary to the case of $\varepsilon = +1$, raising the ECT with $\varepsilon = -1$ will lead to $\theta_t > \theta_n$, and lowering the ECT corresponds to $\theta_t < \theta_n$. The conclusion that $E(\Omega_1) < E(\Omega)$ when $\theta_t < \theta_n$ and Ω lies above Ω_1 (or when $\theta_t > \theta_n$ and Ω lies below Ω_1) still holds true for the case of $\varepsilon = -1$. Therefore, raising and lowering the pressure will lead to the filling and drainage in the ECT for both the cases $\varepsilon = +1$ and $\varepsilon = -1$, respectively. This surprising behaviour implies that the ECT is sensitive to pressure.

3.2. *Critical values* χ_1^* *for* $\varepsilon = \pm 1$

Figure 4 shows the contour lines of χ_1^* (red lines) and the menisci (black lines). As discussed in § 2.3, the critical value χ_1^* is related to the shape of the ECT with $\theta = \pi/2$ by $\chi_1^* = -\tilde{K}_N$. Thus, the points on the line $\chi_1^* = 0$ in figure 4(*a*) are the inflection points of the ECTs with $\theta = \pi/2$ for $\varepsilon = +1$, and there is no inflection point on the ECT with $\theta = \pi/2$ for $\varepsilon = -1$. The contour lines $\chi_1^* = +\infty$ are the envelopes of the solution curves because the envelopes can be seen as ECTs with $\theta = 0$ which have the boundary parameters $\chi_1 = +\infty$.

The critical value χ_1^* can be used to determine the meniscus stability to pressure disturbances. For a simply connected axisymmetric meniscus with arbitrary contact

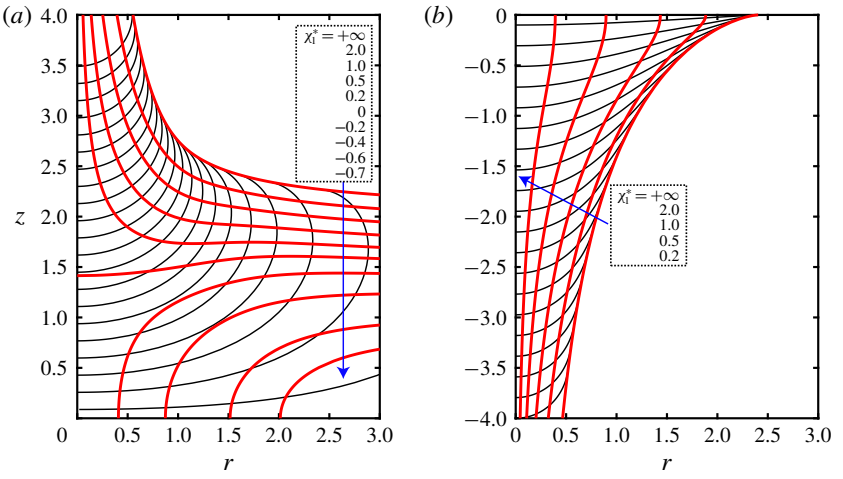

FIGURE 4. Contour lines (red lines) of χ_1^* for (*a*) $\varepsilon = +1$ (see also figure 4 in Zhang & Zhou (2020)) and (*b*) $\varepsilon = -1$. The black lines are the solution curves of the Young–Laplace equation. The values of χ_1^* for the contour lines along the arrow direction are given in each box from top to bottom.

angle θ wetting a solid, the boundary parameter χ_1 is calculated by (2.13) and then is compared to its critical value χ_1^* (i.e. the value at the contact point in figure 4). It is shown that the equilibrium within regions Λ_1 and Λ_2 is stable if $\chi_1 > \chi_1^*$, and is unstable if $\chi_1 < \chi_1^*$ (Slobozhanin & Alexander 2003). It is noted that only the meniscus in the maximal stability regions Λ_1 and Λ_2 can be stable to pressure disturbances because the envelopes (i.e. the boundaries of Λ_1 and Λ_2) correspond to $\chi_1^* = +\infty$.

To illustrate how to determine the meniscus stability by comparing χ_1 and χ_1^*, we examine the stability of the planar meniscus in a vertical straight circular tube with contact angle $\theta = \pi/2$ and radius R for both positive and negative loads. For this configuration, substituting $\tilde{K} = 0$ and $K = 0$ into (2.13) gives the boundary parameter $\chi_1 = 0$. By comparing χ_1 and χ_1^* (see figure 4), it is found that the planar meniscus in the tube with an arbitrary radius R is stable for positive loads and is unstable for negative loads.

4. Conclusions

A mathematical model for determining the general ECT shapes under positive and negative loads has been proposed by following the parameterized Young–Laplace equation (2.1), where the curvatures of the ECTs are determined by the system of ordinary differential equations (2.1) and (2.8). There are five types of ECTs for $\varepsilon = +1$ and three types for $\varepsilon = -1$ (see figure 3). The general ECTs, which are extended from the ordinary ECTs studied by Wente (2011), can be seen as non-uniform circular nozzles connected to a liquid bath which has a constant pressure at the inlet. The ECT has a surprising behaviour whereby lowering the pressure at the ECT inlet slightly from the value $p = -\varepsilon z$ causes the ECT to completely drain out, while raising the pressure slightly forces the ECT to fill up. This surprising behaviour implies that the ECT is sensitive to pressure.

Because the ECTs have a boundary parameter that is equal to the critical value χ_1^*, the curvatures $\tilde{K}_N$ of the ECTs with $\theta = \pi/2$ are related to the critical value by $\chi_1^* = -\tilde{K}_N$. This relation provides a convenient method for calculating the critical value χ_1^* of the boundary parameter for a simply connected axisymmetric meniscus without solving the Jacobi equation (2.10).

Acknowledgement

This research was supported in part by the National Natural Science Foundation of China (no. 11972170).

Declaration of interests

The authors report no conflict of interest.

Appendix A

We know that

$$\left.\frac{\mathrm{d}\psi_r}{\mathrm{d}s}\right|_L = \psi_{rr}\cos\psi + \psi_{rz}\sin\psi. \tag{A 1}$$

Differentiating (2.6*a*) with respect to r gives

$$\frac{\partial}{\partial r}\left(\left.\frac{\mathrm{d}\psi}{\mathrm{d}s}\right|_L\right) = \psi_{rr}\cos\psi + \psi_{rz}\sin\psi - {\psi_r}^2\sin\psi + \psi_r\psi_z\cos\psi. \tag{A 2}$$

Comparing (A 1) and (A 2), one finds

$$\left.\frac{\mathrm{d}\psi_r}{\mathrm{d}s}\right|_L = \frac{\partial}{\partial r}\left(\left.\frac{\mathrm{d}\psi}{\mathrm{d}s}\right|_L\right) + {\psi_r}^2\sin\psi - \psi_r\psi_z\cos\psi. \tag{A 3}$$

Differentiating (2.1*c*) with respect to r, we have

$$\frac{\partial}{\partial r}\left(\left.\frac{\mathrm{d}\psi}{\mathrm{d}s}\right|_L\right) = \frac{\sin\psi - r\psi_r\cos\psi}{r^2}. \tag{A 4}$$

Substituting (A 4) into (A 3), we obtain

$$\left.\frac{\mathrm{d}\psi_r}{\mathrm{d}s}\right|_L = \frac{\sin\psi}{r^2} + \frac{\psi_r\,(\psi_r - \varepsilon z\cos\psi)}{\sin\psi}. \tag{A 5}$$

REFERENCES

BOSTWICK, J. B. & STEEN, P. H. 2015 Stability of constrained capillary surfaces. *Annu. Rev. Fluid Mech.* **47**, 539–568.

BOUCHER, E. A. & EVANS, M. J. B. 1975 Pendent drop profiles and related capillary phenomena. *Proc. R. Soc. Lond.* A **346**, 349–374.

BRAKKE, K. A. 1992 The surface evolver. *Exp. Math.* **1**, 141–165.

CALLAHAN, M., CONCUS, P. & FINN, R. 1991 Energy minimizing capillary surfaces for exotic containers. In *Computing Optimal Geometries* (ed. J. E. Taylor), pp. 13–15. AMS.

CONCUS, P. & FINN, R. 1989 Instability of certain capillary surfaces. *Manuscr. Math.* **63**, 209–213.

CONCUS, P. & FINN, R. 1991 Exotic containers for capillary surfaces. *J. Fluid Mech.* **224**, 383–394.

CONCUS, P., FINN, R. & WEISLOGEL, M. 1992 Drop-tower experiments for capillary surfaces in an exotic container. *AIAA J.* **30**, 134–137.

CONCUS, P., FINN, R. & WEISLOGEL, M. 1999 Capillary surfaces in an exotic container: results from space experiments. *J. Fluid Mech.* **394**, 119–135.

FINN, R. 1986 *Equilibrium Capillary Surfaces*. Springer.

FINN, R. 1988 Non uniqueness and uniqueness of capillary surfaces. *Manuscr. Math.* **61**, 347–372.

GILLETTE, R. D. & DYSON, D. C. 1972 Stability of axisymmetric liquid–fluid interfaces towards general disturbances. *Chem. Engng J.* **3**, 196–199.

GULLIVER, R. & HILDEBRANDT, S. 1986 Boundary configurations spanning continua of minimal surfaces. *Manuscr. Math.* **54**, 323–347.

HUH, C. & SCRIVEN, L. E. 1969 Shapes of axisymmetric fluid interfaces of unbounded extent. *J. Colloid Interface Sci.* **30**, 323–337.

KRAVCHENKO, V. V. & PORTER, R. M. 2010 Spectral parameter power series for Sturm–Liouville problems. *Math. Meth. Appl. Sci.* **33** (4), 459–468.

LAWRENCE, J. D. 2013 *A Catalog of Special Plane Curves*. Courier Corporation.

MYSHKIS, A. D., BABSKII, V. G., KOPACHEVSKII, N. D., SLOBOZHANIN, L. A., TYUPTSOV, A. D. & WADHWA, R. S. 1987 *Low-Gravity Fluid Mechanics*. Springer.

RUSSO, M. J. & STEEN, P. H. 1986 Instability of rotund capillary bridges to general disturbances: experiment and theory. *J. Colloid Interface Sci.* **113**, 154–163.

SIEGEL, D. 1980 Height estimates for capillary surfaces. *Pacific J. Math.* **88**, 471–515.

SLOBOZHANIN, L. A. & ALEXANDER, J. I. D. 2003 Stability diagrams for disconnected capillary surfaces. *Phys. Fluids* **15**, 3532–3545.

SLOBOZHANIN, L. A., ALEXANDER, J. I. D. & RESNICK, A. H. 1997 Bifurcation of the equilibrium states of a weightless liquid bridge. *Phys. Fluids* **9**, 1893–1905.

TSORI, Y. 2006 Discontinuous liquid rise in capillaries with varying cross-sections. *Langmuir* **22**, 8860–8863.

WANG, C. Y. & CHENG, P. 1996 A multiphase mixture model for multiphase, multicomponent transport in capillary porous media – I. Model development. *Intl J. Heat Mass Transfer* **39**, 3607–3618.

WENTE, H. C. 1999 Stability analysis for exotic containers. *Dyn. Contin. Discrete Impuls. Syst.* **5**, 151–158.

WENTE, H. C. 2011 Exotic capillary tubes. *J. Math. Fluid Mech.* **13**, 355–370.

YOUNG, T. III 1805 An essay on the cohesion of fluids. *Phil. Trans. R. Soc. Lond.* **95**, 65–87.

ZHANG, F. & ZHOU, X. 2020 Capillary surfaces in and around exotic cylinders with application to stability analysis. *J. Fluid Mech.* **882**, A28.